Crystal-field theoretical approach to second harmonic generation on antiferromagnetic NiO(001), CoO(001), and FeO(001) surfaces

2005 J. Phys.: Condens. Matter 17 7489

(http://iopscience.iop.org/0953-8984/17/48/003)

INSTITUTE OF PHYSICS PUBLISHING JOURNAL OF PHYSICS: CONDENSED MATTER

J. Phys.: Condens. Matter **17** (2005) 7489–7503 doi:10.1088/0953-8984/17/48/003

Crystal-field theoretical approach to second harmonic generation on antiferromagnetic NiO(001), CoO(001), and FeO(001) surfaces

O Ney[1,3], **M Trzeciecki**[2] **and W Hübner**[1]

[1] Department of Physics, Kaiserslautern University of Technology, Box 3049, D-67653 Kaiserslautern, Germany
[2] Hans Güntner GmbH, Industriestrasse 14, D-82256 Fürstenfeldbruck, Germany

E-mail: oney@physik.uni-kl.de

Received 2 August 2005, in final form 21 October 2005
Published 11 November 2005
Online at stacks.iop.org/JPhysCM/17/7489

Abstract

Using an extended Hubbard model, we calculate the many-body states of various transition-metal (TM) ions in the full spherical symmetry, thus accounting for the electronic correlations in TM oxides (TMOs). The influence of the symmetry of the bulk (cubic) crystal and of an (001) surface is described by a ligand-field procedure. The Slater integrals are fitted to gas phase data, EELS experiments, and low-lying states from *ab initio* theory. We present spectra of second harmonic generation from the bulk states and from the (001) surfaces.

1. Introduction

The current speed of magnetic recording is of the order of nanoseconds, i.e. close to a single precession cycle of the magnetization (Larmor frequency). Achieving a significantly higher speed will require completely new approaches, such as hybrid or optical recording. In order to overcome the deficiencies of the contemporary computer memories and read–write heads of hard disks, both permanent and dynamic, new designs like magnetic random access memories (MRAMs) are under development [1]. They will eliminate the mechanical motion and the hierarchical structure of the contemporary memories and simplify the design of the CPUs. One of the most important components of these MRAMs is tunnelling magnetoresistance (TMR) devices, where the read-out current passing through the device depends on the relative magnetization of two ferromagnetic (FM) layers. The central layer of such a trilayer structure consists of an oxide sandwiched between a soft and a hard magnetic layer (often a ferro-/antiferromagnetic exchange-bias system). Therefore, the performance of these future devices depends heavily on the properties of oxides. Besides, one of the ferromagnetic layers is 'pinned' by an antiferromagnet (exchange bias). Thus, the investigation of antiferromagnetic

[3] Author to whom any correspondence should be addressed.

(AF) oxides (also of their spin dynamics) is of technological importance. In addition, NiO may have advantages as a non-metallic seed layer and also as a magnetic tunnelling barrier. As a further development, nano-oxide structures are proposed in order to replace the whole exchange-biased system of the tunnel junction.

For these applications it is necessary to develop a technique in order to investigate AF oxide surfaces and buried interfaces. Besides, the preparation of TM oxide films is already a challenge and requires a method to characterize the structure and magnetism of these materials. Optical second harmonic generation (SHG) may be such a technique, since conventional linear optical techniques, such as linear magnetic dichroism, if able to see magnetic signals on antiferromagnets at all, quadratically couple to the magnetic order parameter and therefore cannot distinguish them from possibly competing ferromagnetic signals. SHG, which linearly couples to the AF order parameter, has already been proven as a versatile technique for the investigation of ferromagnetism at surfaces, and is also proficient in discriminating AF signals from FM ones. The sensitivity of this technique to volume *antiferromagnetism* has been shown experimentally [2] and explained theoretically [3]. The sensitivity of SHG to *surface* antiferromagnetism has been predicted theoretically [4–6]. The appropriate choice of the experimental geometry enhances the selectivity of this method. One may choose different incoming and outgoing angles and exploit certain combinations of polarizer and analyser angles.

Excited states in TM oxides have always been difficult to access theoretically due to the highly correlated 3d electrons. The localized nature of these optically active states makes them more amenable to theoretical methods usually applied for small clusters rather than to band-structure approaches commonly used for extended solids [7]. In our approach, these pronounced local-symmetry features are addressed by allowing for the full spherical symmetry of the Hamiltonian of a free ion and subsequently lowering the symmetry by the ligand field of the surface. The correlations are taken into account by coupling two, three, and four holes in the 3d and 4s shells. This significant extension of our previous results for the two-hole configuration [4, 8] permits us to compute the electronic many-body structure of the majority of TMOs, in particular also CoO and FeO and their surfaces, thus demonstrating the versatility of our theoretical methods. Previous results of our calculations, already allowing for some technologically important predictions (fast spin dynamics accompanied by a long lasting coherence, laser-driven remagnetization), were presented in [8]. The system addressed in that earlier work, due to the restrictions of the theory to two-hole couplings, was a prototypical Ni^{2+} ion on NiO(001). Now we can address different electronic configurations of various materials with similar structure. In this work, for the sake of consistency, we treat one surface orientation [(001)] and one spin structure of *all three* cubic AF oxides, NiO, CoO, and FeO.

2. Theory

The source of the SHG response is the nonlinear electrical polarization $P_{\mathrm{el}}^{(2\omega)}$ given by

$$P_{\mathrm{el},i}^{(2\omega)} = \epsilon_0 \chi_{ijk}^{(2\omega)} : E_j^{(\omega)} E_k^{(\omega)}. \tag{1}$$

Here, $E^{(\omega)}$ is the electric field of the incident light, while ϵ_0 is the vacuum permittivity and $\chi_{ijk}^{(2\omega)}$ is the nonlinear magneto-optical susceptibility tensor within the electric-dipole approximation. Thus, the calculation of the $\chi_{ijk}^{(2\omega)}$ tensor allows for the prediction of the SHG response of TMO surfaces. The nonvanishing elements of this tensor can be determined, for a given surface structure, by symmetry analysis [4, 5]. To obtain quantitative results, however, an electronic calculation is required, which has been outlined in [8]. Here, we describe this procedure in more detail and extend it to a generalized electronic configuration.

Table 1. The energy levels (in eV) of the Ni^{2+} ion with $3d^2 4s^2$ configuration in the spherical symmetry (see footnote 5).

Hole configurations $3d^2 4s^0$ and $3d^2 4s^2$			
State			Energy for NiO
$E(^1S) = C_{2n}$	$+14B$	$+7C$	7.0677
$E(^3P) = C_{2n}$	$+7B$		*2.1276*
$E(^1D) = C_{2n}$	$-3B$	$+2C$	*1.8370*
$E(^3F) = C_{2n}$	$-8B$		*0.0000*
$E(^1G) = C_{2n}$	$+4B$	$+2C$	*2.8299*
$C_{22} = 1.1038$, $B = 0.1418$, and $C = 0.5639$ for NiO			

In TMO, optical SHG results from the states lying within the optical gap. These states are formed by highly correlated 3d electrons of the metal ion and thus are highly localized. The optical transitions between the 3d states of the TM ion become allowed by the surface symmetry breaking. Charge-transfer excitations to oxygen states start at or above the optical gap, which is 4.3 eV for NiO. Consequently, we limit ourselves to the electronic states localized on the metal ion. First, we determine the states for the spherical symmetry, then we introduce the crystal field, which lowers the symmetry. The surface states of the TM ion are thus determined by a ligand-field method. This *parametrized approach* is general enough to address all the materials which we aim to calculate (NiO, CoO, and FeO). Only the parameters have to be fitted to independent experiments or to results of first-principles calculations specific for each material.

2.1. Two-hole states in the spherical symmetry

We begin with the electronic configuration $3d^8 4s^0$ (corresponding hole configuration $3d^2 4s^2$), which is the ground state configuration of Ni^{2+} in NiO[4]. We have to note that the inclusion of a fully occupied shell (as $4s^2$ here) only shifts the zero of energy (the term C_2 in table 1) but neither affects the energies of the individual states differently nor does it affect the symmetry of the wavefunctions. Thus it suffices to consider partially occupied shells only.

The correlation of d electrons couples the two holes in the d shell of the ion, in the limit of weak spin–orbit coupling, by an LS coupling (neglecting the spin–orbit coupling (SOC)). The resulting coupled states have quantum numbers which are expressed as

$$\begin{aligned} L_z &= l_{z,1} + l_{z,2} \\ S_z &= s_{z,1} + s_{z,2}. \end{aligned} \tag{2}$$

Here, the $l_{z,i}$ and $s_{z,i}$ ($i = 1, 2$) denote the z-components of orbital and spin momenta of the ith hole, respectively. From equation (2) it becomes clear that the orbital momentum of the coupled state constructed from two d holes can be 0, 1, 2, 3, or 4, which is conventionally labelled by the spectroscopic symbols as S, P, D, F, and G. The resulting spin can be equal to zero or unity; in other words, each of these states can have a singlet or triplet spin multiplicity. Since the two holes are indistinguishable, the Pauli principle forbids two identical holes to produce a coupled state. This limitation leaves us with the following set of two-hole states: ^{1}S, ^{3}P, ^{1}D, ^{3}F, and ^{1}G [9]. These spherical-symmetry adapted states are produced from simple

[4] Throughout this work, we assume a transfer of an integer number of electrons to the oxygen atom.

products of d holes with the use of Clebsch–Gordan decomposition

$$\{d_{l=2,s=1/2} \otimes d_{l=2,s=1/2}\}_{L,M,S,S_z} = \sum_{m_1,m_2,s_{z1},s_{z2}} C^{LM}_{2,m_1,2,m_2} \cdot C^{SS_z}_{1/2,s_{z1},1/2,s_{z2}} \cdot d_{2,m_1,1/2,s_{z1}} \cdot d_{2,m_2,1/2,s_{z2}} \tag{3}$$

where d_{l,m,s,s_z} denotes a single-particle basis function defined by the set of quantum numbers l, m, s, s_z and $C^{JM}_{j_1,m_1,j_2,m_2}$ are the Clebsch–Gordan coefficients, followed by a Gram–Schmidt orthonormalization procedure. As a result we obtain orthonormal wavefunctions for these spherical states, expressed as linear combinations of simple antisymmetric products of d-hole wavefunctions (Slater determinants).

The determination of the energy levels for these states requires the solution of the following many-body Hamiltonian:

$$\hat{H}_{sph} = \sum_{i=1}^{N} \hat{U}_i + \frac{1}{2} \sum_{i \neq j}^{NN} \hat{Q}_{ij}, \tag{4}$$

where the one-hole operator $\hat{U}_i$ describes the kinetic energy of the ith particle and its interaction with the nucleus, while the two-hole operator $\hat{Q}_{i,j}$ accounts for the electrostatic Coulomb interaction between different holes, and N is the number of particles that form the many-body states.

The Hamiltonian commutes with all components of the resultant angular momenta **L** and **S**; therefore, there are no matrix components connecting states with different values $\mathbf{L^2}$, $\mathbf{S^2}$, L_z, and S_z. The spin dynamics for the models described later exclusively results from the dephasing due to the quantum nature of the system and has no classical analogue. Note that the energy of the $3d^24s^2$ and $3d^24s^0$ configurations does not depend on the values of L_z and S_z, which means that the states are degenerate.

The energy levels of the states are presented in table 1 (the last column contains the calculated energies for the Ni^{2+} ion in eV).[5] Comparing the values computed within CFT with those provided experimentally gives the possibility to estimate the reliability of CFT results for the materials under consideration.

The common term C_{2n} (which is C_{mn} for the $3d^m4s^n$ configuration) does not depend on the values of L and S and describes the interaction with the nucleus, kinetic energies, and two-particle 3d–4s interactions.

The constants B and C (so-called Racah parameters) result from the interaction of 3d holes. The parameters C_{ij} (where i and j are numbers of 3d and 4s particles in the incomplete shells of the metal ion) are usually referred to as the Racah parameter A. However, we decided to separate C_{ij} from B and C in order to compare the two latter parameters for the systems being explored. They can also be expressed in terms of Slater integrals as $B = F_2(3d, 3d) - 5F_4(3d, 3d)$, and $C = 35F_4(3d, 3d)$.

Knowing the value of these parameters will allow us to determine the energy levels of the $3d^24s^2$ states of a free Ni^{2+} ion. Although the values of these parameters have been found already, we repeated the calculations taking into account experimental results which appeared after the publication [10] and found an agreement with the results presented by Griffith (who estimates $B = 0.134 - 0.137 - 0.129$ and $C = 0.545 - 0.508 - 0.471$ for free ions Ni^{2+}–Co^{2+}–Fe^{2+} accordingly; see tables 1, 2, and 4). The fitting of these parameters is described below.

[5] In tables 1, 2, 3, 4, 8, 9, 10, 11, 12, 13 the energies given in *italic* font denote the energies of levels for fitting the crystal-field theory (CFT) parameters. All the energies in the tables result from CFT while the 'input' energies are given in the text.

Table 2. The energy levels (in eV) of Co^{2+} ion with $3d^3 4s^2$ configuration in the spherical symmetry (see footnote 5).

Hole configurations $3d^3 4s^0$ and $3d^3 4s^2$				
State				Energy for CoO
$E(^2P) = C_{3n}$	$-6B$	$+3C$		2.6928
$E(^4P) = C_{3n}$				*1.8893*
$E(a^2D) = C_{3n}$	$+5B$	$+5C$	$-\alpha$	*2.9576*
$E(b^2D) = C_{3n}$	$+5B$	$+5C$	$+\alpha$	7.2778
$E(^2F) = C_{3n}$	$+9B$	$+3C$		4.5820
$E(^4F) = C_{3n}$	$-15B$			*0.0000*
$E(^2G) = C_{3n}$	$-11B$	$+3C$		*2.0630*
$E(^2H) = C_{3n}$	$-6B$	$+3C$		*2.6928*
$\alpha = \sqrt{193B^2 + 4C^2 + 8BC}$				
$C_{32} = 1.9020$, $B = 0.1260$, and $C = 0.5197$ for CoO				

Table 3. The energy levels (in eV) for the Ni^{2+} ion with $3d^3 4s^1$ configuration in the spherical symmetry (see footnote 5).

Hole configuration $3d^3 4s^1$					
State					Energy for NiO
$E(^1P) = C_{31}$	$-6B$	$+3C$			10.5283
$E(a^3P) = C_{31}$	$-6B$	$+3C$	$-2G$		*9.7994*
$E(b^3P) = C_{31}$			$+G$		10.0413
$E(^5P) = C_{31}$			$-3G$		*8.8253*
$E(a^1D) = C_{31}$	$+5B$	$+5C$		$-\alpha_2$	10.8461
$E(b^1D) = C_{31}$	$+5B$	$+5C$		$+\alpha_2$	15.8678
$E(a^3D) = C_{31}$	$+5B$	$+5C$	$-2G$	$-\alpha_2$	10.3590
$E(b^3D) = C_{31}$	$+5B$	$+5C$	$-2G$	$+\alpha_2$	15.3808
$E(^1F) = C_{31}$	$+9B$	$+3C$			12.7086
$E(a^3F) = C_{31}$	$-15B$		$+G$		*7.6192*
$E(b^3F) = C_{31}$	$+9B$	$+3C$	$-2G$		12.2215
$E(^5F) = C_{31}$	$-15B$		$-3G$		*6.6451*
$E(^1G) = C_{31}$	$-11B$	$+3C$			9.8017
$E(^3G) = C_{31}$	$-11B$	$+3C$	$-2G$		*9.3146*
$E(^1H) = C_{31}$	$-6B$	$+3C$			10.5284
$E(^3H) = C_{31}$	$-6B$	$+3C$	$-2G$		10.0413
$G = G_2(4s; 3d)$, $\alpha_2 = \sqrt{193B^2 + 8BC + 4C^2}$					
$C_{31} = 9.5558$, $B = 0.1453$, $C = 0.6149$, and $G = 0.2435$ for NiO					

2.2. Three-hole states

Next, we construct the three-hole states (i.e. the states of the electronic configurations $3d^7 4s^0$ and $3d^7 4s^2$ or corresponding hole configurations $3d^3 4s^2$ and $3d^3 4s^0$), of which the first one is used to treat the Co^{2+} ion. We do this by coupling the third d hole to the previously obtained $3d^2 4s^0$ states, using again the Clebsch–Gordan scheme. There are 120 resulting three-hole states conveniently grouped as ^2P, a^2D, b^2D, ^2F, ^2G, ^2H, ^4P, and ^4F according to their degeneracy in the spherical environment.

Table 4. The energy levels (in eV) of the Fe^{2+} ion with $3d^4 4s^2$ configuration in the spherical symmetry (see footnote 5).

Hole configurations $3d^4 4s^0$ and $3d^4 4s^2$				
State				Energy for FeO
$E(a^1S) = C_{4n}$	$+10B$	$+10C$	$-\alpha_1$	*4.3318*
$E(b^1S) = C_{4n}$	$+10B$	$+10C$	$+\alpha_1$	12.2004
$E(a^3P) = C_{4n}$	$-5B$	$+5.5C$	$-\alpha_2$	*2.6397*
$E(b^3P) = C_{4n}$	$-5B$	$+5.5C$	$+\alpha_2$	*6.2114*
$E(a^1D) = C_{4n}$	$+9B$	$+7.5C$	$-\alpha_3$	*4.5766*
$E(b^1D) = C_{4n}$	$+9B$	$+7.5C$	$+\alpha_3$	9.3753
$E(^3D) = C_{4n}$	$-5B$	$+4C$		*3.7205*
$E(^5D) = C_{4n}$	$-21B$			*0.0000*
$E(^1F) = C_{4n}$		$+6C$		*5.2357*
$E(a^3F) = C_{4n}$	$-5B$	$+5.5C$	$-\alpha_4$	*2.6912*
$E(b^3F) = C_{4n}$	$-5B$	$+5.5C$	$+\alpha_4$	*6.1600*
$E(a^1G) = C_{4n}$	$-5B$	$+7.5C$	$-\alpha_5$	*3.7296*
$E(b^1G) = C_{4n}$	$-5B$	$+7.5C$	$+\alpha_5$	*7.0017*
$E(^3G) = C_{4n}$	$-12B$	$+4C$		*2.9154*
$E(^3H) = C_{4n}$	$-17B$	$+4C$		*2.3402*
$E(^1I) = C_{4n}$	$-15B$	$+6C$		*3.5104*
$\alpha_1 = \sqrt{772B^2 + 16C^2 + 32BC}$				
$\alpha_2 = \sqrt{228B^2 + 2.25C^2 - 6BC}$				
$\alpha_3 = \sqrt{324B^2 + 2.25C^2 + 18BC}$				
$\alpha_4 = \sqrt{153B^2 + 2.25C^2 + 9BC}$				
$\alpha_5 = \sqrt{177B^2 + 2.25C^2 - 3BC}$				
$C_{42} = 2.4457$, $B = 0.1150$, and $C = 0.4700$ for FeO				

At this stage two different levels characterized by the same set of quantum numbers appear. This leads to non-diagonal matrix elements between the states a^2D and b^2D. Their energies have to be found from the secular equation. Because of this two ^{2}D levels have a $\mp\alpha$ term in the expressions for their energies.

The results for this configuration are presented in table 2.

The wavefunctions (eigenfunctions of the Hamiltonian) for the two ^{2}D levels may only be found if the values of parameters C_{32}, B, and C are known.

In order to describe the electronic configuration $3d^7 4s^1$ (e.g., an excited state of Ni^{2+} in NiO) we must account for the single hole in the 4s shell. This is done by coupling this hole to the $3d^3 4s^0$ states using the Clebsch–Gordan procedure. The obtained states differ from the original three-hole states by the total spin number, while the other quantum numbers remain unchanged, which leads to additional splittings (described via the parameter G in table 3) of the $3d^3 4s^0$ states. The energy levels for these states are the solutions of the Schrödinger equation with the Hamiltonian (4).

The parameters used here are the same as in the previous case of two holes in the d shell (except for G). The fitting of these parameters will be described below. Please note that in this case the appearance of terms characterized by the same values of **L** and **S** is due to the addition of the spin angular momentum (one s particle), while the energies depend on the value of **L**. Thus there are analytical solutions (contain no square root) for the energies of the states a^3P, b^3P, a^3F, and b^3F which do not have non-linear α-terms.

Table 5. Experimentally measured energies (in eV) for ions in gas phase.

NiO^{2+}		CoO^{2+}		FeO^{2+}	
$3d^84s^0$		$3d^74s^0$		$3d^64s^0$	
^3F	0.0000	^4F	0.0000	^5D	0.0000
^1D	1.7398	^4P	1.8849	a^3P	2.4060
^3P	2.0658	^2G	2.1051	^3H	2.4861
^1G	2.8652	^2H	2.8171	a^3F	2.6611
$3d^74s^1$		a^2D	2.8591	^3G	3.0450
^5F	6.6587			^1I	3.7639
a^3F	7.6055			^3D	3.8097
^5P	8.8116			a^1G	3.8296
^3G	9.3146			a^1S	4.3164
a^3P	9.8130			a^1D	4.4393
				^1F	5.3188
				b^3P	6.0939
				b^3F	6.2224
				b^1G	7.0949

2.3. Four-hole states

The spherical-symmetry states of the Fe^{2+} ground state in FeO and highly excited states in NiO which belong to the electronic configurations $3d^64s^2$ and $3d^64s^0$ (hole configurations $3d^44s^0$ for NiO^{2+} and $3d^44s^2$ for FeO^{2+}) are obtained by coupling another d hole to the three-hole states calculated previously (the electronic configuration $3d^74s^1$ of CoO^{2+}, which gives energies higher than the optical gap, is neglected in this work). The resulting states are given in table 4.

The energy levels for these states are obtained by solving the Hamiltonian (4). The resulting energy levels can be completely expressed in terms of the previously employed parameters.

Comparing the energies in tables 4 and 5 we may conclude that CFT gives rather poor agreement for the Fe ion, and, as will be seen later, for the bulk as well as for the (001) surface of FeO. Because of this discrepancy we decided to present these results to show the limits of CFT but will not use them further.

2.4. Fitting of the energy parameters

In order to obtain the numerical values of the energy levels of the ions in the spherical environment we fit the values of all previously described parameters to gas phase experiments [11] (table 5).

Having fitted the parameters B, C, and G as well as the prefactors C_{ij} (note that they are different from values for charge-zero metal atoms in ferromagnetic metals), we can express the energies and the wavefunctions of all states of spherical symmetry. Note that, for all the ions, the $3d^{N+1}4s^1$ states (where $N = 2, 3, 4$ for Ni^{2+}, Co^{2+}, FeO^{2+}) lie far above the optical gap, therefore their influence on SHG is of minor importance and we will omit them in the following consideration.

It is also important that the values of B and C for NiO fitted to two independent electronic configurations are almost the same, which *a posteriori* justifies the use of CFT.

3. Gap states in a crystal symmetry

In the previous section, we have calculated the many-body states of a TM ion in a spherically symmetric environment. Here, we use crystal-field theory to obtain the wavefunctions and energy levels in the cubic (O_h) environment of the bulk crystal[6].

The lower symmetry of a cubic crystal or of the surface lowers the degeneracy of most of the states, i.e. causes level splitting. Here, we address this splitting in a ligand-field approach, calculating the crystal-field related levels.

The crystal field is added to the Hamiltonian described in equation (4):

$$\hat{H} = \hat{H}_{sph} + \hat{V}_{\mathrm{lig}}. \tag{5}$$

This field acts on the individual states, changing their energies:

$$E_{\mathrm{lig}} = \langle\Psi|\hat{H}_{sph}|\Psi\rangle + \langle\Psi|\hat{V}_{\mathrm{lig}}|\Psi\rangle. \tag{6}$$

The detailed description of the crystal-field method is given in [12]. Here we consider a metal ion surrounded by six (in the bulk) or five (on the (001) surface assuming perfect bulk termination) oxygen ions (point charges Ze), positioned at the distance R from the metal ion. The potential V_{lig} of the crystal field is given as ($N = 5$ or 6):

$$V_{\mathrm{lig}}(\mathbf{r}) = \sum_{i=1}^{N} \frac{Ze^2}{|\mathbf{R}_i - \mathbf{r}|}. \tag{7}$$

After expansion of V_{lig} in terms of Legendre polynomials and application of the addition theorem for spherical harmonics we arrive at the following form of V_{lig} for 3d and 4s particles (terms up to the fourth order):

$$V_{\mathrm{lig}}^{\mathrm{O_h}} = \frac{6Ze^2}{R}C_0^{(0)} + r^4\frac{Ze^2}{R^5}\left\{\frac{7}{2}C_4^{(0)} + \frac{\sqrt{70}}{4}\left(C_4^{(-4)} + C_4^{(4)}\right)\right\} \tag{8}$$

$$V_{\mathrm{lig}}^{\mathrm{C_{4v}}} = \frac{5Ze^2}{R}C_0^{(0)} + r^4\frac{Ze^2}{R^5}\left\{\frac{5}{2}C_4^{(0)} + \frac{\sqrt{70}}{4}\left(C_4^{(-4)} + C_4^{(4)}\right)\right\} - r^2\frac{Ze^2}{R^3}C_2^{(0)} - r\frac{Ze^2}{R^2}C_1^{(0)} - r^3\frac{Ze^2}{R^4}C_3^{(0)}, \tag{9}$$

where

$$C_k^{(m)} = C_k^{(m)}(\theta\phi) = \left(\frac{4\pi}{2k+1}\right)^{1/2} Y_{km}(\theta\phi). \tag{10}$$

The inversion symmetry is broken on the (001), surface which leads to the appearance of odd-order terms in $V_{\mathrm{lig}}^{\mathrm{C_{4v}}}$. Although these terms do not contribute to the multiplet energies, they do allow electric-dipole transitions (parity forbidden in the centrosymmetric bulk) between the levels and thus may lead to an SHG signal from the surface.

The one-particle energies under the action of this field are presented in table 6, where

$$a = \frac{Ze^2}{R}, \tag{11}$$

$$b = \frac{1}{7}\frac{Ze^2}{R^3}\langle r_{3\mathrm{d}}^2\rangle, \tag{12}$$

$$c = \frac{1}{42}\frac{Ze^2}{R^5}\langle r_{3\mathrm{d}}^4\rangle, \tag{13}$$

$$\langle r_{nl}^k\rangle = \int \mathrm{d}r\, r^{2+k}|R_{nl}(r)|^2. \tag{14}$$

[6] We neglect the tiny rhombohedral distortion of the TMOs in the antiferromagnetic phase and in the C_{4v} symmetry of an (001) surface.

Table 6. One-particle energy matrix elements under the action of the crystal field V_{lig}; see the definitions in equations (11)–(13).

	Bulk	Surface
$\langle\phi_{3d\pm2}\|V_{\mathrm{lig}}\|\phi_{3d\pm2}\rangle$	$6a + 7c$	$5a + 2b + 5c$
$\langle\phi_{3d\pm1}\|V_{\mathrm{lig}}\|\phi_{3d\pm1}\rangle$	$6a - 28c$	$5a - b - 20c$
$\langle\phi_{3d0}\|V_{\mathrm{lig}}\|\phi_{3d0}\rangle$	$6a + 42c$	$5a - 2b + 30c$
$\langle\phi_{3d\pm2}\|V_{\mathrm{lig}}\|\phi_{3d\mp2}\rangle$	$35c$	$35c$

These are the so called ligand-field parameters, where a describes the energy shift in an isotropic crystal field (zero-order term in V_{lig}), c in the O_h symmetry, and b and c in the C_{4v} symmetry, respectively[7]. The energies of the 4s particles are not split due to the crystal field.

3.1. Bulk states

Group theory tells us that, in the cubic environment, states are not characterized any more by the quantum numbers γLS (where γ denotes different levels having the same values of L and S), but are labelled in terms of the irreducible representations $\gamma\Gamma S$ (where $\Gamma = A_{1g}, A_{2g}, E_g, T_{1g}, T_{2g}, A_{1u}, A_{2u}, E_u, T_{1u}, T_{2u}$) of L in the point group O_h. As the first step we have to adapt the previously computed wavefunctions for spherical symmetry by using cubic harmonics presented in table 7. However, some of the states appear more than once in the configuration, which leads to the off-diagonal elements of the energy matrix, connecting the states with equal ΓS. The additional index γ distinguishes them. These off-diagonal elements may be neglected if the crystal-field strength is small enough compared to the electronic interaction, because of their relatively small influence on the resulting states. Nevertheless, in the current work we treat them exactly and diagonalize the energy matrices. This is a great improvement over our previous calculations, in which we used the CFT diagonal-sum rule and did not consider off-diagonal elements at all [13].

In principle, knowing the position of the ligands for a particular material, and possibly approximating the ligands by point charges, we can calculate the crystal-field parameters. Instead we use the available theoretical and experimental results for low lying states [14, 15] (and references therein) and fit these parameters so that the energies of the already known states are expressed correctly.

To fit the CFT parameters we use the energies for NiO, collected from the literature [16]. They are (in eV) $^3A_{2g} = 0.0000$, $^3T_{2g} = 0.8406$, $a^3T_{1g} = 1.4586$, $^1E_g = 1.8474$, $a^1T_{2g} = 2.5553$, $b^3T_{1g} = 2.8186$. The resulting states for NiO bulk are presented in table 8.

The energies (in eV) used to fit the parameters for CoO given in [17] are $a^4T_{1g} = 0.0000$, $a^4T_{2g} = 0.6800$, $a^2E_g = 1.9000$, $a^2T_{1g} = 2.5100$, $a^2T_{2g} = 2.5500$, and $^4A_{2g} = 1.4100$. The results are given in table 9.

The energies (in eV) used to fit the parameters for FeO are $^5T_{2g} = 0.0000$, $^5E_g = 1.0400$, $a^3T_{1g} = 1.7200$, and $a^1A_{1g} = 2.0200$ eV are taken from [15]. The results are in table 10. The fit quality decreases going from NiO via CoO to FeO.

3.2. Surface states

The statements in the previous paragraphs for the surface are also applicable to the bulk with the only difference that Γ may be A_1, A_2, B_1, B_2, or E for the symmetry group C_{4v} (this group does not contain inversion, thus subscripts g and u disappear). Experimental energies for NiO

[7] The parameters a, b, and c are different from the indices $\gamma = a, b, \ldots$ used to distinguish states with equal LS (ΓS).

Table 7. Simplified cubic harmonics ($L_m^+ = \sqrt{\frac{1}{2}}(L_m + L_{-m})$, $L_m^- = \sqrt{\frac{1}{2}}(L_m - L_{-m})$).

Free ion	Cubic state	Cubic harmonics		
S	A_{1g}	S_0		
P	T_{1g}	P_{-1}	P_0	P_1
D	E_g	D_0	D_2^+	
	T_{2g}	D_2^-	D_{-1}	D_1
F	A_{2g}	F_2^-		
	T_{1g}	F_0	$\sqrt{\frac{5}{8}}F_{-3} + \sqrt{\frac{3}{8}}F_1$	$\sqrt{\frac{5}{8}}F_3 + \sqrt{\frac{3}{8}}F_{-1}$
	T_{2g}	F_2^+	$\sqrt{\frac{3}{8}}F_{-3} - \sqrt{\frac{5}{8}}F_1$	$\sqrt{\frac{3}{8}}F_3 - \sqrt{\frac{5}{8}}F_{-1}$
G	A_{1g}	$\sqrt{\frac{5}{12}}G_4^+ + \sqrt{\frac{7}{12}}G_0$		
	E_g	$\sqrt{\frac{7}{12}}G_4^- - \sqrt{\frac{5}{12}}G_0$	G_2^+	
	T_{1g}	G_4^-	$\sqrt{\frac{1}{8}}G_{-3} + \sqrt{\frac{7}{8}}G_1$	$\sqrt{\frac{1}{8}}G_3 + \sqrt{\frac{7}{8}}G_{-1}$
	T_{2g}	G_2^-	$\sqrt{\frac{7}{8}}G_{-3} - \sqrt{\frac{1}{8}}G_1$	$\sqrt{\frac{7}{8}}G_3 - \sqrt{\frac{1}{8}}G_{-1}$
H	E_g	H_2^-	H_4^-	
	T_{1g}	H_0	$\sqrt{\frac{63}{128}}H_{-5} + \sqrt{\frac{35}{128}}H_3 + \sqrt{\frac{15}{64}}H_{-1}$	$\sqrt{\frac{63}{128}}H_5 + \sqrt{\frac{35}{128}}H_{-3} + \sqrt{\frac{15}{64}}H_1$
	T_{1g}	H_4^+	$\sqrt{\frac{5}{128}}H_{-5} - \sqrt{\frac{81}{128}}H_3 + \sqrt{\frac{21}{64}}H_{-1}$	$\sqrt{\frac{5}{128}}H_5 - \sqrt{\frac{81}{128}}H_{-3} + \sqrt{\frac{21}{64}}H_1$
	T_{2g}	H_2^+	$\sqrt{\frac{15}{32}}H_{-5} - \sqrt{\frac{3}{32}}H_3 - \sqrt{\frac{7}{16}}H_{-1}$	$\sqrt{\frac{15}{32}}H_5 - \sqrt{\frac{3}{32}}H_{-3} - \sqrt{\frac{7}{16}}H_1$
I	A_{1g}	$\sqrt{\frac{7}{8}}I_4^+ - \sqrt{\frac{1}{8}}I_0$		
	A_{2g}	$\sqrt{\frac{5}{16}}I_6^+ - \sqrt{\frac{11}{16}}I_2^+$		
	E_g	$\sqrt{\frac{1}{8}}I_4^+ + \sqrt{\frac{7}{8}}I_0$	$\sqrt{\frac{11}{16}}I_6^+ + \sqrt{\frac{5}{16}}I_2^+$	
	T_{1g}	I_4^-	$\sqrt{\frac{11}{32}}I_{-5} + \sqrt{\frac{15}{32}}I_3 - \sqrt{\frac{3}{16}}I_{-1}$	$\sqrt{\frac{11}{32}}I_5 + \sqrt{\frac{15}{32}}I_{-3} - \sqrt{\frac{3}{16}}I_1$
	T_{2g}	I_2^-	$\sqrt{\frac{165}{256}}I_{-5} - \sqrt{\frac{81}{256}}I_3 + \sqrt{\frac{5}{128}}I_{-1}$	$\sqrt{\frac{165}{256}}I_5 - \sqrt{\frac{81}{256}}I_{-3} + \sqrt{\frac{5}{128}}I_1$
	T_{2g}	I_6^-	$\sqrt{\frac{3}{256}}I_{-5} + \sqrt{\frac{55}{256}}I_3 + \sqrt{\frac{99}{128}}I_{-1}$	$\sqrt{\frac{3}{256}}I_5 + \sqrt{\frac{55}{256}}I_{-3} + \sqrt{\frac{99}{128}}I_1$

Table 8. Bulk energies (in eV) of NiO computed within CFT (see footnote 5).

$^3A_{2g}$	*0.0000*	^1E_g	*2.1356*	$^3T_{1g}$	*3.1706*	$^1T_{1g}$	3.6467	$^1T_{2g}$	4.2451
$^3T_{2g}$	*0.8168*	$^1T_{2g}$	*2.8722*	$^1A_{1g}$	3.3471	^1E_g	4.1649	$^1A_{1g}$	8.1841
$^3T_{1g}$	*1.4075*								

$a = 0.0720$, $c = -0.0117$

(from [14], in eV) are $^3B_1 = 0.0000$, $a^3E = 0.6500$, $^3B_2 = 1.0000$, $^3A_2 = 1.3000$, and $b^3E = 1.4400$. The resulting states for the NiO(001) surface are given in table 11.

At this point we see again that the values of the crystal-field parameters are very similar for two independent fits (bulk and surface), as can be seen comparing the tables 8 and 11.

The parameters obtained in this way allow for the determination of the energy shifts caused by the symmetry breaking, and thus for the determination of the energy levels of the surface. This gives us the full knowledge about the wavefunctions (eigenfunctions of Hamiltonian) and corresponding energies of states at the (001) surface of NiO.

Table 9. Bulk energies (in eV) of CoO computed within CFT (see footnote 5).

$^4T_{1g}$	*0.0000*	$^2T_{1g}$	*2.2329*	$^2T_{1g}$	2.8161	$^2T_{2g}$	3.6590	$^2T_{1g}$	5.0521
$^4T_{2g}$	*0.5681*	$^2T_{2g}$	*2.2354*	$^2T_{2g}$	3.0758	$^2T_{1g}$	3.6619	$^2A_{2g}$	5.1501
$^4A_{2g}$	*1.2393*	$^4T_{1g}$	2.3541	$^2T_{1g}$	3.1293	^2E_g	3.6851	$^2T_{2g}$	7.7899
^2E_g	*1.7612*	$^2A_{1g}$	2.6310	^2E_g	3.3476	$^2T_{2g}$	4.9821	^2E_g	7.7981

$a = 0.0328$, $c = -0.0096$

Table 10. Bulk energies (in eV) of FeO computed within CFT (see footnote 5).

^5E_g	*0.0000*	$^3T_{1g}$	3.0368	$^1A_{1g}$	*3.6746*	$^1A_{1g}$	5.0467	$^1A_{1g}$	7.0434
$^5T_{2g}$	*0.4807*	^3E_g	3.1371	$^1T_{1g}$	3.7583	$^1T_{2g}$	5.0623	$^1T_{1g}$	7.1728
$^3T_{1g}$	*2.1297*	$^3T_{1g}$	3.2140	^3E_g	3.9188	$^1T_{1g}$	5.4945	^1E_g	7.2952
^3E_g	2.4009	$^1T_{2g}$	3.3231	$^1T_{2g}$	4.0376	$^1T_{2g}$	5.5738	$^1T_{2g}$	7.6115
$^3T_{1g}$	2.5627	^1E_g	3.3405	$^3T_{2g}$	4.0924	$^1A_{2g}$	5.6385	$^1T_{2g}$	9.5921
$^3T_{2g}$	2.5799	$^3T_{1g}$	3.4528	^1E_g	4.1237	$^3T_{1g}$	6.3101	^1E_g	9.8224
$^3A_{2g}$	2.7763	$^3T_{2g}$	3.5077	$^1A_{1g}$	4.4086	$^3T_{2g}$	6.5332	$^1A_{1g}$	12.5232
$^3A_{1g}$	2.9154	$^1A_{2g}$	3.5883	$^1T_{1g}$	4.4938	$^3A_{2g}$	6.5555		
$^3T_{1g}$	2.9154	$^1T_{2g}$	3.6620	^1E_g	4.5732	$^3T_{1g}$	6.6362		

$a = -0.0049$, $c = 0.0069$

Table 11. The energy levels (in eV) of the Ni^{2+} ion on the (001) surface of NiO computed within CFT (see footnote 5).

$^3B_1$	*0.0000*	^3E	*1.4615*	$^1B_2$	2.9333	$^3A_2$	3.7000	^1E	4.5158
^3E	*0.6945*	$^1A_1$	1.9728	^3E	3.1331	$^1B_1$	3.7821	$^1A_1$	4.7614
$^3B_2$	*1.0208*	$^1B_1$	2.1036	$^1A_1$	3.3764	$^1B_2$	3.9732	$^1A_1$	8.3387
$^3A_2$	*1.2921*	^1E	2.7424	^1E	3.4000	$^1A_2$	4.4751		

$a = 0.1036$, $b = 0.1926$, $c = -0.0146$

Table 12. The energy levels (in eV) of the Co^{2+} ion on the (001) surface of CoO computed within CFT (see footnote 5).

$^4A_2$	*0.0000*	$^2B_1$	2.2688	^2E	2.6778	^2E	3.8500	^2E	5.8016
^4E	*0.1370*	$^2B_2$	2.3464	^2E	2.8383	$^2A_2$	4.2767	$^2A_1$	7.3305
$^4B_2$	*0.2601*	^2E	2.3562	^4E	3.2409	^2E	4.4766	^2E	7.9234
$^4B_1$	0.3910	$^4A_2$	2.4542	$^2B_2$	3.2868	$^2A_1$	4.5481	$^2B_1$	9.1996
^4E	*0.6539*	$^2A_2$	2.5112	$^2A_2$	3.4292	$^2B_2$	5.0355	$^2B_2$	9.6423
^2E	1.9290	$^2B_2$	2.5129	$^2B_1$	3.4476	$^2B_1$	5.3264		
$^2A_1$	2.0786	$^2B_1$	2.5815	^2E	3.4782	^2E	5.4669		
$^2A_2$	2.1402	$^2A_1$	2.5966	$^2A_1$	3.7509	$^2A_2$	5.6167		

$a = 0.0263$, $b = 0.3763$, $c = 0.0093$

The experimentally known energies (in eV) for the (001) surface of CoO are [18]: $a^4A_2 = 0.0000$, $a^4E = 0.0500$, $^4B_2 = 0.3500$, and $b^4E = 0.7000$. Results of our calculations are in table 12. Although the convergence of the resulting energies to their experimental values is less good than the one for NiO, the results are still of a good quality since the CFT method gives the proper order of levels and acceptable differences between 'input' and 'output' energies in CFT. In our opinion, these differences show a fair applicability of CFT to CoO.

The energies for the (001) surface of FeO obtained in cluster calculations [15] are: $a^5E = 0.0000$, $a^5B_2 = 0.1300$, $a^5A_1 = 0.4700$, and $a^5B_1 = 1.1400$ eV. Results of our

Table 13. The energy levels (in eV) of the Fe^{2+} ion on the (001) surface of FeO computed within CFT (see footnote 5).

^5E	*0.0000*	$^3A_2$	2.8845	$^3B_2$	3.9018	^1E	4.8421	^3E	7.2204
$^5B_2$	*0.2184*	^3E	3.0232	^1E	3.9257	$^1A_1$	5.1080	$^1B_2$	7.2361
$^5A_1$	*0.5584*	$^1A_2$	3.0976	^3E	3.9545	$^1B_1$	5.2987	$^1A_2$	7.5717
$^5B_1$	*1.1653*	^3E	3.2457	$^3A_2$	4.0445	$^1A_1$	5.4704	$^1A_1$	7.6124
^3E	1.7334	$^3B_1$	3.2535	$^1B_1$	4.0564	^1E	5.5207	$^1B_1$	7.6911
$^3B_2$	1.9895	$^3A_1$	3.3103	$^1A_1$	4.0657	$^1B_1$	5.7329	^1E	7.7652
$^3A_2$	2.0447	$^3B_2$	3.3180	^3E	4.2097	$^1B_2$	5.8541	$^1A_1$	7.8681
^3E	2.3276	^3E	3.3251	$^1A_2$	4.2110	^1E	5.8913	$^1A_1$	9.3361
$^3A_2$	2.2737	$^1B_2$	3.4558	^1E	4.3398	$^1A_2$	5.9807	$^1B_1$	9.8059
$^1A_1$	2.3422	$^1B_1$	3.4613	$^1B_2$	4.4016	^3E	6.2927	^1E	9.9376
^3E	2.4973	^1E	3.5139	$^1A_1$	4.4777	$^3B_1$	6.4380	$^1B_2$	10.3288
$^3B_1$	2.7265	$^1B_2$	3.6396	$^3A_1$	4.5070	^3E	6.4508	$^1A_1$	12.7796
^3E	2.7291	$^3A_2$	3.6621	$^1B_1$	4.5592	$^3A_2$	6.7527		
$^3B_2$	2.8167	$^3A_1$	3.7119	$^3B_1$	4.5696	$^3B_2$	6.7965		
^1E	2.8484	$^3B_1$	3.7285	^1E	4.5911	$^3A_2$	6.9618		
$^3A_1$	2.8628	$^1A_1$	3.7913	$^1B_2$	4.7426	^1E	7.1254		

$a = 0.0154$, $b = -0.1179$, $c = -0.0135$

calculations are given in table 13. Unfortunately, the computed levels are not comparable with the reference values. Even the proper symmetry of the ground state cannot be reproduced. Thus we have reached the point where CFT fails. In our opinion, this is due to the smaller number of electrons in the outermost shell. Compared with NiO and CoO the 3d shell in FeO (consisting of six electrons) is far from being closed. In this case electronic correlations between these electrons in the solid may differ from the ones for the free ion. Thus, the parameters describing the Coulomb interaction for the free ion change their values already in the bulk material. The other reason for this might be an inconsistency between CFT and cluster calculations, which is very difficult to check experimentally because of the instability of FeO against further oxidation which leads to the formation of Fe_2O_3 (thus precluding the reliable measurements of the interfacial properties).

We have also tried to use the quantum chemistry results [19] for NiO as reference energies in CFT and found a somewhat less good agreement compared with the experimental reference energies presented above. Although quantum chemistry (in contrast to DFT-based methods) is able to give the comparable values of the optical gap as well as intragap multiplet states, it overestimates their values. However, the analysis in [19] shows that higher order correlations are desired in order to improve the *ab initio* description of strongly correlated systems.

4. SHG

CFT results, presented before, allow us to compute the nonlinear optical susceptibility tensor $\chi^{(2\omega)}$. According to the general theory presented in [20] this tensor can be computed as

$$\chi^{(2\omega)}_{ijk}(2\mathbf{q}, 2\omega) = \frac{-\mathrm{i}e^3}{2q^3\Omega} \cdot \sum_{\mathbf{k},l,l',l''} \langle \mathbf{k}+2\mathbf{q}, l''|\mathrm{e}^{2\mathrm{i}\mathbf{q}\cdot\mathbf{r}}|\mathbf{k}, l\rangle\langle \mathbf{k}, l|\mathrm{e}^{-\mathrm{i}\mathbf{q}\cdot\mathbf{r}}|\mathbf{k}+\mathbf{q}, l'\rangle \times \langle \mathbf{k}+\mathbf{q}, l'|\mathrm{e}^{-\mathrm{i}\mathbf{q}\cdot\mathbf{r}}|\mathbf{k}+2\mathbf{q}, l''\rangle \times \frac{\frac{f(\mathbf{E}_{\mathbf{k}+2\mathbf{q},l''},t)-f(\mathbf{E}_{\mathbf{k}+\mathbf{q},l'},t)}{E_{\mathbf{k}+2\mathbf{q},l''}-E_{\mathbf{k}+\mathbf{q},l'}-\hbar\omega+\mathrm{i}\hbar\alpha} - \frac{f(\mathbf{E}_{\mathbf{k}+\mathbf{q},l'},t)-f(\mathbf{E}_{\mathbf{k},l},t)}{E_{\mathbf{k}+\mathbf{q},l'}-E_{\mathbf{k},l}-\hbar\omega+\mathrm{i}\hbar\alpha}}{E_{\mathbf{k}+2\mathbf{q},l''} - E_{\mathbf{k},l} - 2\hbar\omega + 2\mathrm{i}\hbar\alpha}. \quad (15)$$

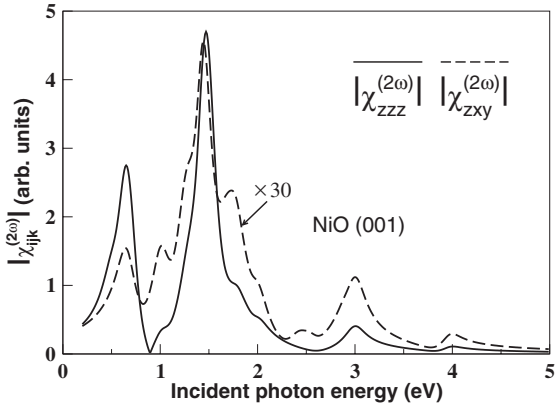

Figure 1. Static dependence of $\chi^{(2\omega)}_{ijk}$ on the frequency of the incident laser for the NiO(001) surface.

It is clearly seen from this equation that the incident laser frequency ω should be adjusted to the resonances of the system. This expression is modified towards a CFT basis set; namely, the one-particle basis set is replaced by the many-particle one provided by CFT, the summations over bands replaced by summations over multiplet levels, and summation in the **k**-space transformed into the integration over the real space. Because CFT fails to give acceptable results for FeO, we concentrate here on NiO and CoO.

Setting the time t equal to zero and choosing unity for the ground state occupancy in equation (15) we are able to study the frequency-dependent response of the sample. There are three ingredients needed for our calculations of the nonlinear susceptibility tensor elements: the wavefunctions of the NiO many-body eigenstates, the transition matrix elements between these states, and the energy levels of these states. The corresponding energies were presented in the previous sections. However, a reliable calculation of the transition matrix elements would require an *ab initio* theory of static and dynamic optical phenomena, which is unfeasible so far (the material class of transition metal oxides is one of the most difficult quantum systems due to their strong electronic correlations). Instead, we will use the approximation of constant transition matrix elements, with selection rules allowing for distinguishing the tensor elements.

Here, we present the spectra of two tensor elements: the prototypic paramagnetic tensor element $\chi^{(2\omega)}_{zzz}$ and the prototypic antiferromagnetic tensor element $\chi^{(2\omega)}_{zxy}$ in figure 1. In both spectra, all computed features fall within the gap, which we assume to be at 4.0 eV for the oxide surfaces[8]. The dominant structure in both spectra corresponds to the transitions from the ground state to the states located near $2\hbar\omega = 3.0$ eV; see table 11. The position of the peak around 1.5 eV corresponds to the fact that the tensor describes SHG. Other, smaller peaks related to transitions between various states are also present. Another feature of the calculated spectra is that the tensor elements are complex and their phases vary. This has important consequences for the AF domain imaging using SHG. It would be highly desirable to compare with a surface SHG experiment [21].

The main distinctive features of the spectrum of the AF tensor element $\chi^{(2\omega)}_{zxy}$ are additional peaks at 1.02, 1.73, and 2.46 eV, where at best shoulders exist in the spectrum of the paramagnetic tensor element $\chi^{(2\omega)}_{zzz}$. Consequently, this is an 'antiferromagnetic' spectral line, which we suppose is especially suitable for nonlinear magneto-optics. Note that the

[8] In general, the surface gap is smaller than that of the bulk due to the reduced coordination number.

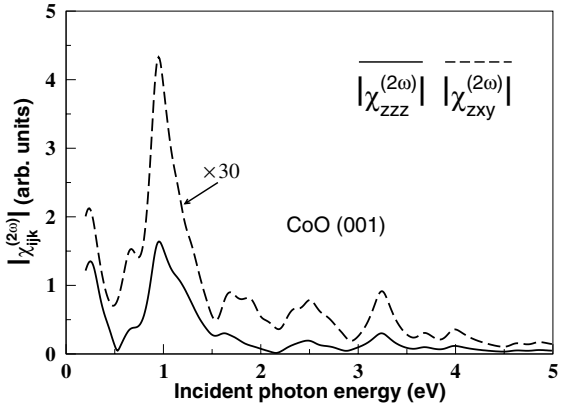

Figure 2. Static dependence of $\chi^{(2\omega)}_{ijk}$ on the frequency of the incident laser for the CoO(001) surface.

AF SHG tensor element $\chi^{(2\omega)}_{zxy}$ is *linear* in the AF order parameter. Although magnetic and nonmagnetic tensor elements differ in magnitude, they can be distinguished in experiment, which is a favourable condition for AF domain imaging. Taking into account the magnitudes of both tensor elements presented in this section, the domain contrast should be comparable to the one in ferromagnets (where it is of the order of *unity* in SHG, as opposed to the small domain contrast in the linear magneto-optical Kerr effect), which suggests an SHG process to be used as a detection technique for the nonlinear magneto-optical response.

Using the results provided by CFT for the (001) surface of CoO, we have computed in the same way the prototypical paramagnetic and antiferromagnetic tensor elements for this system. The results are shown in figure 2. The presence of an additional unpaired electron in the 3d shell leads to a bigger number of levels within the gap and the structure of these tensor elements for CoO is more complicated. However, there are characteristic features which allow us to distinguish the contributions of $\chi^{(2\omega)}_{zzz}$ from those of $\chi^{(2\omega)}_{zxy}$. Most of these features appearing above the main peak (around 1 eV) make it more difficult to access them experimentally. However, the possible bunching of levels can make up for the disadvantage of their large number.

5. Conclusions, outlook

The electronic structure of transition metal oxides NiO, CoO, and FeO and their (001) surfaces is described by means of the CFT, which efficiently handles the systems whose behaviour is mostly determined by strongly correlated electrons of the outermost incomplete shell (here 3d electrons). Using CFT results, measurable features of TMOs are computed, namely the nonlinear optical susceptibility tensor. In order to find the appropriate laser frequency we compute the dependence of typical magnetic and crystallographic elements of $\chi^{(2\omega)}$ on the frequency of the incident light. There exist frequencies for which these tensor elements have different behaviours, which means that the laser pulse of a specially chosen frequency allows us to identify the magnetic state of the surface. Dynamical SHG of antiferromagnetic spectral lines show ultrafast spin dynamics [13]. Long lasting coherence together with the possibility of ultrafast (of the order of femtoseconds) spin switching makes these materials very promising for technological applications, such as permanent magnetic storage devices and quantum computing. Recently, the quantum beating effects on the picosecond timescale

in bulk NiO were shown experimentally [22], with the coherence time exceeding 100 ps. Until now, among solids, only semiconductors and nuclear spins have been known to exhibit the combination of these features, suffering however from a much slower dynamics. Moreover, NiO possesses a high density of permanent magnetic moments (like metals), which is an option for device size reduction. Comparing NiO and CoO, we may conclude that the former one is more suitable for nonlinear optics. Although the bigger number of levels lying within the gap of CoO may suppress well pronounced peaks in the SHG signal (unless bunching of intragap levels occurs) this material is a good candidate for the experiment on spin dynamics. In addition to the fact that we were not able to get a proper theoretical description of FeO within CFT, one may suspect more difficulties with this material in a nonlinear optical experiment due to its nonstoichiometric behaviour.

A more detailed first principles description of nonlinear optical phenomena requires further theoretical investigations as well as experimental measurements [21]. In particular, the relativistic effects as well as a treatment of the interaction with a high intensity laser field are of importance.

Acknowledgments

The authors acknowledge the financial support provided by the Forschergruppe 'Oxidische Grenzflächen' (project number 404), Deutsche Forschungsgemeinschaft (priority programmes SPP 1133 and SPP 1153), EU RTN-networks EXCITING and DYNAMICS, and Landesschwerpunkt MINAS.

References

[1] de Boeck J and Borghs G 1999 *Phys. World* (April) 27
[2] Fiebig M, Fröhlich D, Krichevtsov B B and Pisarev R V 1994 *Phys. Rev. Lett.* **73** 2127
[3] Muthukumar V N, Valentí R and Gros C 1995 *Phys. Rev. Lett.* **75** 2766
[4] Trzeciecki M, Dähn A and Hübner W 1999 *Phys. Rev.* B **60** 1144
[5] Trzeciecki M and Hübner W 1999 *Appl. Phys.* B **68** 473
[6] Dähn A, Hübner W and Bennemann K H 1996 *Phys. Rev. Lett.* **77** 3929
[7] Radwanski R J and Ropka Z 2004 *Preprint* cond-mat/0404713
[8] Trzeciecki M, Ney O, Zhang G P and Hübner W 2001 *Adv. Solid State Phys.* **41** 547
[9] Trzeciecki M 2000 Second harmonic generation from antiferromagnetic interfaces *PhD Thesis* Martin-Luther-Universitaet Halle-Wittenberg
[10] Griffith J S 1961 *The Theory of Transition-Metal Ions* (Cambridge: Cambridge University Press)
[11] Moore C E 1971 *Atomic Energy Levels NBS Circular* vol II (Washington, DC: US Govt Printing Office)
[12] Sugano S, Tanabe Y and Kamimura H 1970 *Multiplets of Transition-Metal Ions in Crystals* (New York: Academic)
[13] Ney O, Trzeciecki M and Hübner W 2002 *Appl. Phys.* B **74** 741
[14] Fromme B 2001 *d–d Excitations in Transition-Metal Oxides: A Spin-Polarized Electron Energy-Loss Spectroscopy (SPEELS) Study* (*Springer Tracts in Modern Physics* vol 70) (Heidelberg: Springer)
[15] Razumov M G and Chugreev A L 2000 *Russ. J. Phys. Chem.* **74** 78
[16] Mackrodt W C and Noguera C 2000 *Surf. Sci.* **457** L386
[17] de Graaf C, de Jong W A, Broer R and Nieuwpoort W C 1998 *Chem. Phys.* **237** 59
[18] Haßel M, Kuhlenbeck H, Freund H-J, Shi S, Freitag A, Staemmler V, Lütkehoff S and Neumann M 1995 *Chem. Phys. Lett.* **240** 205
[19] Satitkovitchai K, Pavlyukh Y and Hübner W 2003 *Phys. Rev.* B **67** 165413
[20] Hübner W and Bennemann K H 1989 *Phys. Rev.* B **40** 5973
[21] Fiebig M, Fröhlich D, Lottermoser Th, Pavlov V V, Pisarev R V and Weber H-J 2001 *Phys. Rev. Lett.* **87** 137202 (this experiment addresses SHG from bulk NiO)
[22] Duong N P, Satoh T and Fiebig M 2004 *Phys. Rev. Lett.* **93** 117402